

Modeling sediment transport on the storage capacity and life prediction of Sadpara dam

Munawwar Ali Abbas ^a, Ahmad Cho ^a, Muhammad Abid ^{b, c, *}, Hafiz Abdul Wajid ^d, Muhktar Ahmed ^e

^a Department of Mathematics University of Baltistan Skardu

^b Interdisciplinary Research Center, COMSATS University Islamabad, Wah Campus, GT Road Wah Cantt, Pakistan

^c UNESCO Chair on Knowledge Systems for IWRM, COMSATS University Islamabad, Wah Campus, GT Road, Wah Cantt, Pakistan

^d Department of Electrical Engineering, Islamic University of Madinah, Saudi Arabia

^e Department of Agronomy, Pir Mehr Ali Shah-Arid Agriculture University Rawalpindi, Pakistan

* Corresponding author: Muhammad Abid, Email: drabid@ciitwah.edu.pk

Received: 22 December 2024, Accepted: 27 March 2025, Published: 01 April 2025

KEY WORDS

HEC – RAS Model
Sediment transport
Reservoir sedimentation
Sadpara River
Storage capacity

ABSTRACT

This study aims to determine storage capacity and life prediction of Sadpara reservoir based on the sediment deposition considering in flow and discharge rate during 2012 to 2021. The main river and reservoir flows and sediments are modelled using the HEC-RAS 5.0.7 software. Ackers-White equation for sediments, continuity and momentum equations to conserve mass and external pressure on the fluid and Toffaletti equation for the sediment load are used. Manning variation of 0.03, 0.035, 0.04 various river stations and Toffaletti grain-size validity range of 0.062mm to 4mm is observed. From model a runoff flow from the valleys on either side of the reservoir observed is almost 2.8% of the total average annual sediment load of 26.9 tones. In addition, more than 50% of the sediment is observed deposited in the upper part of the reservoir which increased with the increased rainfall. The volume of water released from the Deosai River, bed slop, and the manning coefficient are concluded the contributing factors for transported sediment deposition in the reservoir. The model presented is recommended beneficial for the prediction of potential changes in the river bathymetry till 2060.

1. Introduction

According to Morris et al. [1], yearly, 0.5% to 1% of the 6,800 km³ of water held in reservoirs is lost globally due to sedimentation. As a result, global per capita reservoir storage capacity drastically decreased around 1980. Nevertheless, the amount of storage available today is comparable to that of around 60 years ago. The roughly 6000 [km]³ gross storage capacity of the world's reservoirs and the yearly reservoir sedimentation as examined by (Sumi and Hirose, 2009). (Basson,2008), investigated that silt

deposition will cause reservoir capacity worldwide to decline by 64% by 2050. The likelihood of flood damage has increased due to storage depletion. (Hosseini K et al., 2015), projected that the movement of runoff, which can be brought on by wind, rain, or snowmelt, is the first step in the sedimentation process. The reservoirs function as silt traps thanks to their high-water flow rates. A review and research perspectives on the mid-reach sediment generation resulting in the sedimentation of reservoirs are given by (Fox et al., 2016). (Lai, S. Y., and Capart, H., 2009)

conclude that the production from erosion of stream banks and gullies is a factor in sediment yield in reservoirs' uneven dependency on the catchment's geophysical and thermodynamic characteristics. Rivers frequently contain a wide range of particles (Fan, J., and Morris, 1992) that enter the reservoir as suspended loads and coarser sediments depending on the material delivered flow velocity and turbulence. (Juracek, 2015) demonstrates the geomorphic phases of a reservoir's existence, showing that the Grading of the silt and sediment deposition inside the reservoir are intimately related. (Capart et al., 2009) stated that Central Taiwan's Wushe reservoir of the Choushui River demonstrates that delta propagation can undergo dramatic evolutions depending based on hydrology, channel design, and sediment properties (Fig. 3a), where the delta advanced 15% of the 4.5 km, which is roughly the length of the reservoir, in two months. Fig. 3b illustrates the migration of a Gilbert-type delta into the Sadpara reservoir. According to (Sloff et al., 1997) sedimentation processes result in reservoirs losing their capacity, which poses a severe danger to their ability to store, utilize, and regulate river runoff.

A few lab tests and outdoor (Park JH et al., 2011) observations are utilized to assess and validate the numerical model since a rise in the sediment load may decrease the river's water quality. Light transmission, fish gill obstruction, and, in difficult situations, river depth, is all negatively impacted by the movement of toxins (Park JH et al., 2011, Nu-Fang et al., 2011). According to (Nu-Fang et al, 2011) a rise in the amount of silt that rivers carry causes surface water quality to decline. Understanding the processes involved in transporting suspended particles is essential for regulating the rate of soil erosion. Maintaining reservoir storage capacity has aided several national goals, claim (Podolak et al., 2015). The study noted that reservoir sedimentation might be stopped by active management of sediment strategies. (White, 2010) addressed the factors influencing the effectiveness and viability of sediment flushing through reservoirs. Sedimentation can decrease hydropower generation by decreasing reservoir storage and resulting in mechanical damage, according to (Obialor et al., 2019). Recent studies (2023–2024) highlight advancements in sediment transport modelling using HEC-RAS (Dahal, V et al.,). A 2023 study in Naumure Multipurpose Project (NMP) reservoir watershed demonstrated HEC-RAS 1D's effectiveness in analysing sediment accumulation upstream of dams. Similarly, a 2024 study in Nepal's Naumure Project forecasted sediment deposition over decades, aiding reservoir management (Kunwar, S et al.,). (Mazhar et al., 2021) discussed the rainfall and

temperature data for the 1980–2017 catchment area of the Tarbela Dam. Additionally, from 2007 to 2012, this study examines the seasonal impacts of silt loads entering the reservoir. Research also emphasizes precise boundary conditions, such as in Pakistan's 2019 Tarbela Reservoir study. The findings showed that the pattern of sediment deposition indicates higher bed elevation at range lines 7–12, which are close to the Main Embankment Dam. Further (Abid et al., 2010) the Tarbela reservoir's tiny tributaries' flow was obstructed at their mouths because of sediment buildup and delta formation. This way, produced pools further limit reservoir capacity. Tarbela Lake's annual average sediment inflow was 265 Mt (Metric Tons). (Rahman, 2005) studied that the Tarbela River has an average annual flow of 64 MAF (78.9 Bm³), primarily because of snow and glacier melt. Because of rising silt levels, a cup-shaped bed profile forms before the tunnel intakes. The Indus River transports massive amounts of silt at one of the fastest known rates in the literature (Meybeck, 1976). Sediments migrating above the bed layer are suspended loads whose weight is carried by water flow and kept suspended in water for an extended period (Haghiabi, 2012). Sediment buildup in lakes causes a wide range of issues. For instance, sediment buildup in lakes reduces the lake's storage capacity, causes navigation issues, and other issues with water quality and the environment (El-Sammany, and El-Moustafa, 2011). It is crucial to evaluate the sediment capacity (quantity) and distribution in lakes to solve the issues caused by sediment buildup and use of the sediment. This will help determine the lakes' capacity and the safest route for boaters to take around the lakes (Abdel-Aziz, 2001).

A lake's operating plan and management greatly depend on the assessment of silt deposition in the lake (El-Moattassem et al., 2005). Different regions of the world have conducted assessments of the sediment capacity of lakes has been studied by (Mandwar et al., 2013). They evaluated the silt buildup in the Totla Doh reservoir. (Schultz, 1997) assessed erosion and sedimentation rates in Lake Kemnade's upper area in Germany. (Issa et al., 2014) analysed the Mosul dam reservoir's sedimentation mechanism in Iraq. Similarly, few more investigations can be viewed in the available references (Lo Curzio et al., 2013, Biggs et al. 2022, Behrangi et al., 2014, Ren et al., 2021).

Considering the above, the present study aims to analyse the underlying causes of sedimentation and find the total amount of sedimentation in Sadpara Dam Skardu, Pakistan. Further, it has also been discussed the effect of flow rate and its effect on sedimentation. The mathematical equation used to analyze these

parameters are the continuity, momentum, and Equation of Toffaletti. The continuity equation describes the transport fluid, showing how a fluid conserves mass while moving. The resultant force a stream of flowing fluid exerts on the boundaries of a flow passage as the flow varies is calculated using the momentum equation. Finally, the Toffaletti equation is used to find the total amount of sediments.

2. Materials and Methods

The continuity equation describes the transfer of some quantities, such as fluid or gas. The continuity equation explains the mass conservation of a fluid in motion. The momentum equation is utilized in open channel flow issues to identify unidentified forces acting at the flow passage's limits as a stream of fluid changes direction or forms a bed in the control volume. While the momentum equation relates velocity and pressure, the continuity equation relates density and speed. To find field variables in a flow field, such as velocity, pressure, etc., we must concurrently solve the continuity and momentum equations (also known as the equation of motion).

2.1 Continuity Equation

Consider the straightforward volume control in (Fig. 5). This Fig. shows the measurement of distance x beside the waterway. $Q(x,t)$ and AT denote the flow and total flow area at the center of the control volume. The active zone A and the off-channel storage area S make up the overall flow area. For a one-dimensional system, the continuity equation describes the conservation of mass. The equation for continuity that results from the addition of the storage term is

$$\frac{\partial A}{\partial t} + \frac{\partial S}{\partial t} + \frac{\partial Q}{\partial x} - q_1 = 0 \quad \text{Eq. (A.1)}$$

2.2 Momentum Equation

Newton's second law describes how to conserve momentum as

$$\sum F_x = \frac{d\bar{M}}{dt} \quad \text{Eq. (A.2)}$$

According to the principle of conservation of momentum, the rate at which momentum builds up in a control volume must match the sum of the net rates at which momentum enters and exits the volume. This vector equation is being used in the x -axis. The fluid mass times the flow-direction velocity equals the momentum flux (MV). We will consider three forces. The first three forces are pressure, gravity, and boundary drag or friction. (Fig. 5) is a general illustration of a cross-section with an uneven cross-section under pressure. The cross-sectional pressure area product is the integral of the total pressure force.

The gradient of pressure is thought to should hydrostatic (pressure varies linearly with depth).

The force of pressure at any location can be expressed as

$$F_p = \int_0^h \rho g(h-y)T(y)dy \quad \text{Eq. (A.3)}$$

The total pressure forces for the control volume:

$$F_{pn} = F_p - \frac{\partial F_p}{\partial x} \frac{\Delta x}{2} - \left(F_p + \frac{\partial F_p}{\partial x} \frac{\Delta x}{2} \right) + F_B \quad \text{Eq. (A.4)}$$

Momentum (Motion) flux: The volume's overall external stresses plus the momentum flux's net rate of entry into the volume is

$$\rho \Delta x \frac{\partial Q}{\partial t} = -\rho \frac{\partial QV}{\partial x} \Delta x - \rho gA \frac{\partial h}{\partial x} \Delta x - \rho gA \frac{\partial z_o}{\partial x} \Delta x - \rho gAS_f \Delta x \quad \text{Eq. (A.5)}$$

The momentum equation's final form is obtained as

$$\frac{\partial Q}{\partial t} + \frac{\partial QV}{\partial x} + gA \left(\frac{\partial z}{\partial x} + S_f \right) = 0 \quad \text{Eq. (A.5)}$$

2.3 Manning's Equation

To determine the flow in an open channel and account for friction losses, use Manning's equation and explain the relationship between conduit velocity and slope-related geometry.

$$Q = \frac{1.49}{n} * A * R^{\frac{2}{3}} * S^{\frac{1}{2}} \quad \text{Eq. (A.6)}$$

Where,

Flow Rate = Q (cfs)

Manning's Ruggedness, n Coefficient (unitless)

Flow Area = A (sf)

Hydraulic Radius, or R

S = Energy Gradient's (ft/ft) Slope

Manning's roughness coefficient (0.040 - 0.050) is employed in Manning's equation to compute channel flow. (Table 5)

2.4 Equation of Toffaletti

Individual sediment transport rates are computed for each zone, and the sum is used to get the overall transport rate. Toffaletti created the equations for each zone using the estimated Rouse concentration profile across the water column and the computed hydraulic factors driving sediment transport. This method is fundamentally different from bed load transport equations (e.g., Wilcock-Crowe equation and Meyerpeter and Muller equation). This study addresses Sadpara Dam's sedimentation challenges by integrating localized geological, hydrological, and operational data into advanced models like Toffaletti's equation and HEC-RAS. The Toffaletti equation is

more suited for channels in sand beds. It enhances precision through creative adjustments, such as refined parameter tuning and the use of Manning's equation for improved flow calculations. The study provides detailed insights into sediment deposition rates, spatial distribution, and impacts on reservoir operations and storage capacity. The following general transport equations apply to a single grain size in the lower, middle, upper, and bed zones:

For Lower Zone

$$g_{ssL} = M \frac{\left(\frac{R}{11.24}\right)^{1+n_v-0.756z} - (2d_m)^{1+n_v-0.756z}}{1+n_v-0.756z} \quad \text{Eq. (A.7)}$$

For Middle zone

$$g_{ssM} = M \frac{\left(\frac{R}{11.24}\right)^{0.244z} \left[\left(\frac{R}{2.5}\right)^{1+n_v-z} - \left(\frac{R}{11.24}\right)^{1+n_v-z} \right]}{1+n_v-z} \quad \text{Eq. (A.8)}$$

For Upper Zone

$$g_{ssU} = M \frac{\left(\frac{R}{11.24}\right)^{0.244z} \left(\frac{R}{2.5}\right)^{0.5z} \left[R^{1+n_v-1.5z} - \left(\frac{R}{2.5}\right)^{1+n_v-1.5z} \right]}{1+n_v-1.5z} \quad \text{Eq. (A.9)}$$

For bed zone

$$g_{sb} = (2d_m)^{1+n_v-0.756z} \quad \text{Eq. (A.10)}$$

$$M = 43.2C_L(1+n_v)VR^{0.756-n_v} \quad \text{Eq. (A.11)}$$

$$gs = g_{ssL} + g_{ssM} + g_{ssU} + g_{sb} \quad \text{Eq. (A.12)}$$

Where:

g_{ssL} = Transport of suspended silt in the lower zone, expressed in per day and feet

g_{ssM} = Transport of suspended sediment in the middle zone is measured in tonnes per day per feet

g_{ssU} = Transport of sediment in the upper zone is measured in tonnes per day per feet

g_{sb} = Transport of bed load sediment in tons per day per feet

gs stands for total sediment transport in tons/day/foot.

M is a parameter for sediment concentration.

C_L stands for the lower zone's sediment content.

R is hydraulic radius

d_m is median particle diameter.

n_v = Exponent of temperature

The relationship between the hydraulic characteristics of the sediment is described by the exponent z .

The researcher must choose the most appropriate method from among the many available for calculating fall velocity. There are four fall velocity

editor methods in HEC-RAS. This investigation made use of the Rubey formula. "Stoke's law" governs the fall velocity for small particles only susceptible to viscous resistance. An impact formula governs the fall velocity for large particles outside of Stoke's area. Rubey created an analytical link between the fall velocity, fluid, and sediment parameters.

$$\omega = F_1 \sqrt{(s-1)gd_s} \quad \text{Eq. (A.13)}$$

In which

$$F_1 = \sqrt{\frac{2}{3} + \frac{36v^2}{gd^3(s-1)}} + \sqrt{\frac{36v^2}{gd^3(s-1)}}$$

Where: ω particles falling velocity; v = viscosity of kinematic; s = particle specific gravity; d = size of the particles (diameter) g = gravitational constant;

F_1 = The Froude Number.

2.5 Case study description

A zoned earth fill embankment of 128 ft high and 560 ft long make up the Main Dam. The project's other key components are a gated spillway with a 5000-cusec capacity, an outlet structure made of RCC concrete conduit, a control tower, a valve, and an irrigation valve. This study presents globally applicable strategies for reservoir sedimentation management by integrating local data with HEC-RAS and Toffaleti's equation. It offers a repeatable framework for accurate sediment modelling through calibration and real-data validation. Insights into sediment deposition patterns support sustainable practices in sediment-prone regions like glacial or monsoonal areas. The findings contribute to international efforts in sedimentation control and reservoir sustainability, making it a valuable resource worldwide. The development of four cascade powerhouses is planned. Steel penstock transports water from the outflow structure to the Powerhouse-1. Water is delivered to Powerhouse-2 through open channels, forebay, and steel penstock. Just downstream of Powerhouse-1, a weir on Satpara nallah directs water to the headrace channel of Powerhouse-2. Powerhouses 1 and 2 started operating in October 2007 and December 2008, respectively. Powerhouses 3 and 4 will begin construction in the middle of this year. Midway through 2023, power houses 3 and 4 will start operating. The Sadpara project, which generated 57 GWh of power by December 2010, is advancing Skardu's trade, industry, and way of life. A Diversion Weir along Sadpara Nallah, Left Bank Canal (135 cusecs), Right Bank Canal (50 cusecs), and their distributaries and minors comprise the irrigation system. The work is 77.5% finished, and the left bank canal is 16 km long, while the right bank canal is roughly 12 km long. The irrigation system will serve a total of around 15,000

acres of land. Table 1 provides the RBC, LBC, and monthly reservoir operation plan. The managed supplies of the project are currently benefiting a sizable chunk of these territories.

Table 1

Silent Features of the reservoir operation plan

| | | | | | | |
|-------------|-------------------------------|---|-------------------------|--|--|---|
| Powerhouses | Installed Capacity 17 MW | Command Area: 10,131 acres total (41.00 km ²) | Dam type: Earth Fill | Spillways: Length of spillway: 1,075 ft. 50-foot spillway width | Reservoir Dimensions (Capacity) Gross storage 93310 Acres ft | Canal Length: Left Bank Canal: 59,000 feet long. |
| | Mean Annual Energy 106 GWh | 8,119 acres make up Left Bank Canal (32.86km ²) | Dam length: 560ft | Capacity of the spillway: 5000 ft ³ /s | Live storage 55617 Acres ft | 30,000 ft Right Bank Canal |
| | No of Powerhouses 4 | | Maximum Height 128ft | | | |

Type of Turbines
Francis
Ability to generate
electricity:
17.366 MW

Table 2

The total Proposed Releases out of Sadpara's Reservoir, the Irrigation Water Supply (IWS) from various sources, Crops Irrigation Water Requirement (CIWR).

| M | IWS and CIWR to 12,316 acres of LBC | | | 3184-acre CIWR and IWS to RBC Area | | S. R releases water for | | |
|-----|-------------------------------------|---------|--------|------------------------------------|-------|-------------------------|----------------|----------|
| | R. of Sadpara | sources | CIWR | IWS | CIWR | IWS of Dam | Domestics use, | Domestic |
| | Flow Discharge(cfs) | | | | | | | |
| Jan | - | 18.22 | - | 1.00 | 1.00 | - | 60.00 | 41 |
| Feb | - | 18.82 | - | 0.94 | 0.94 | - | 60.00 | 41 |
| Mar | 45.667 | 19.37 | 65.02 | 1.86 | 16.82 | 14.96 | 103.48 | 41 |
| Apr | 99.333 | 21.77 | 121.04 | 1.21 | 31.31 | 30.10 | 160.00 | 41 |
| Ma | 48.612 | 131.74 | 138.85 | 21.67 | 41.26 | 25.71 | 136.99 | 41 |
| Jun | 21.934 | 209.72 | 148.74 | 66.91 | 38.46 | 10.54 | 140.38 | 41 |
| Jul | 13.901 | 157.82 | 94.29 | 73.59 | 24.38 | 6.68 | 135.17 | 41 |
| Aug | 10.421 | 116.44 | 70.70 | 26.70 | 18.28 | 5.01 | 83.13 | 41 |
| Sep | 9.591 | 83.65 | 65.02 | 19.95 | 16.81 | 4.61 | 75.15 | 41 |
| Oct | 3.842 | 32.301 | 26.03 | 5.62 | 6.73 | 1.84 | 52.30 | 41 |
| Nov | - | 24.26 | - | 1.09 | - | - | 60.00 | 41 |
| Dec | - | 17.75 | - | 1.13 | - | - | 60.00 | 41 |
| Avg | 91.21 | 70.98 | 31.66 | 24.25 | 18.47 | 12.43 | 93.88 | 41 |

Table 3

An illustration of a software menu showing sediment data

| Function | D | dm | s | V | W | T | d | S |
|----------------|-----------|-----------|----------|-----------|----------|-------|----------|------------------|
| Ackers-White | 0.01-1.4 | NA | 1.0-2.7 | 0.07-7.1 | 0.23-4.0 | 46-89 | 0.04-7.0 | 0.00006-0.037 |
| Englund-Hansen | 0.19-1.33 | 0.19-0.93 | NA | 0.65-6.34 | NA | 45-93 | NA | 0.000055-0.019 |
| Laursen | 0.67-54 | 0.08-0.7 | NA | 0.068-7.8 | 63-3640 | 32-93 | NA | 0.0000021-0.0018 |
| Laursen | 0.03-3.6 | 0.011-29 | NA | 0.7-9.4 | 0.25-6.6 | 46-83 | NA | 0.00025-0.025 |
| Meyer-Peter | 0.03-3.9 | NA | 1.25-4.0 | 1.2-9.4 | 0.5-6.6 | NA | 0.4-29 | 0.0004-0.02 |

| | | | | | | | | |
|---------------------|-----------|------------|----|---------|-----------|-------|-----------|-----------------|
| Tofaletti | 0.07-56.7 | 0.095-0.76 | NA | 0.7-7.8 | 63-3640 | 32-93 | 0.062-4.0 | 0.000002-0.0011 |
| Tofaletti | 0.07-0 | 0.45-0.91 | NA | 0.7-6.3 | 0.8-8 | 40-93 | 0.06-0.4 | 0.00014-0.019 |
| Yang (field-sand) | 0.04-0 | NA | NA | 0.8-6.4 | 0.44-1750 | 32-94 | 0.15-1.7 | 0.000043-0.028 |
| Yang (field-gravel) | 0.08-0. | NA | NA | 1.4-5.1 | 0.44-1750 | 32-94 | 2.5-7.0 | 0.0012-0.029 |

Table 4

Coefficients for some commonly used surface materials:

| Surface material | The Manning's Roughness Coefficient is n. |
|----------------------------|---|
| Earth's smooth coefficient | 0.018 |
| Clean Earth Channel | 0.022 |
| Gravelly Earth Channel | 0.025 |
| Earth channel-weedy | 0.030 |
| Mountain River | 0.040 - 0.050 |

Table 5

Daily flow rate of few days of the Sadpara river.

| Simulation time | Flow Time (hourse) | Flow (cfs) |
|-----------------|--------------------|------------|
| 22 Jul 2014 | 24 | 508 |
| 29 Jul 2014 | 24 | 510 |
| 05Aug 2015 | 24 | 511 |
| 15Aug 2015 | 24 | 514 |
| 02 Jul 2016 | 24 | 515 |
| 19 Jul 2016 | 24 | 516 |
| 26Aug 2017 | 24 | 517 |
| 29Aug 2017 | 24 | 508 |
| 22 Jul 2018 | 24 | 501 |
| 29 Jul 2018 | 24 | 502 |

2.6. Geometry Of The Problem

2.6.1. Cross sections

The schematic river system is created by connecting the river cross sections along the entire reach using geometric data in HEC-RAS. At River Station, there was the greatest upstream cross-section. (Rs) 42000, and the most downstream cross section was at Rs 1050. (A). About 50 meters separate the river stations on average. For each cross-section, the data primarily contain stations and elevations. In addition, additional information is needed, such as the lengths of the main channel, the right-over bank, and the left-over bank's downstream reaches (ROB). Input data needed to produce the geometric data file include Manning's

values for LOB, channel, and ROB and contraction and extraction coefficients.

2.6.2. Water surface profiles calculations

The one-dimensional energy and continuity equations must be solved to determine one-dimensional steady stream (steady flow) and surface profiles of the water. Then, using elements of the energy equation, depicted in (Fig. 9) The water surface profiles are computed using HEC-RAS from one section to the next.

2.6.3. Quasi-unsteady flow

One must be familiar with the Hydraulic River to use HECRAS to calculate the transit of silt. HEC-RAS frequently uses many sediment flow models, including hydrodynamic simplification. Three unique time steps are used by HEC-RAS, each of which is a subdivision of the other. To calculate sediment movement. Each unique steady flow profile is split into smaller time blocks that are then split again. The computation's hourly increment, flow's hourly duration, and flow (m³/s) for an upstream external barrier must be considered when choosing a flow series; see (Table 5). For each downstream region, potential boundaries include Normal Depth, Rating Curve, or Stage Time Series. A "Rating Curve" was the downstream boundary condition in this study's research. Possible rating curve.

3. Results and Discussion

3.1 Sedimentation And Its Effects On Dam

A reservoir's storage capacity is significantly impacted by sediment influx. Many reservoirs worldwide are plagued by the threat of sedimentation with higher flow and subsequent drop in flow speed resulting in a loss in the reservoir's volume for transporting material, which in turn causes most incoming sediments to settle. The likelihood of flood damage has increased due to storage depletion. Therefore, it is important to reduce sediment loads through various methods as it will restore and enhance aquatic habitats, navigation, electricity, irrigation, and reduce flood damage. (Fig. 2a) shows the sedimentation deposited in the Sadpara reservoir at the end of the summer season. Dam safety is impacted by sedimentation, which lowers the

capability for energy production, storage, discharge, and flood attenuation. As a result, the load on the dam and gates is increased, mechanical equipment is damaged, and various environmental effects are produced. (Fig. 2b) shows the effect of floods on the Sadpara reservoir.

It was emphasized that preserving reservoir storage capacity has helped achieve a few national goals. The study noted that reservoir sedimentation might be stopped by active management of sediment strategies. Deposited sediments in reservoirs can severely affect the environment and the security of dams. Therefore, designing, building, and operating sustainable hydropower projects in developing areas must consider sediment management practices.

3.2 Flow And Data

The Deosai river flow influx served as the reservoir's main sediment supply. It can be seen from (Fig. 3b) that several primary valleys feed the reservoir with water. The total Proposed Releases out of Sadpara's Reservoir, the Irrigation Water Supply (IWS) from various sources, Crops Irrigation Water Requirement (CIWR) are displayed in Table 2. Data required for HEC-RAS4 to calculate sediment load are mentioned in (Table 3). The massive Sadpara River is 4 km long and the longest river in Skardu. This river has two major branches one is the Deosai, and another one is the Sadpar broq streams which meet at mail pain (Sadpara village). After the model was calibrated for flow simulation, the sediment transportation inside the reservoir are simulated, and the sediment data and graph are shown in (Fig. 4) and (Table 4).

3.3 HEC – RAS and Mathematical Calculations

(Fig. 5) is the control volume for the momentum and continuity equation's derivation. This figure shows the measurement of distance x beside the waterway. $Q(x, t)$ and AT denote the flow and total flow area at the center of the control volume. The active zone A and the off-channel storage area S make up the overall flow area. According to the principle of conservation of momentum, the rate at which momentum builds up in a control volume must match the sum of the net rates at which momentum enters and exits the volume. This vector equation is being used in the x -axis. The fluid mass times the flow-direction velocity equals the momentum flux (MV). We will consider three forces. The first three forces are pressure, gravity, and boundary drag or friction. (Fig. 6) is a general illustration of a cross-section with an uneven cross-section under pressure. The cross-sectional pressure area product is the integral of the total pressure force. To determine the flow in an open channel and account for friction losses, use Manning's equation and explain

the relationship between conduit velocity and slope-related geometry.

Individual sediment transport rates are computed for each zone, and the sum is used to get the overall transport rate. Toffaletti created the equations for each zone using the estimated Rouse concentration profile across the water column and the computed hydraulic factors driving sediment transport. This method is fundamentally different from bed load transport equations. They use the sediment shear stresses to compute movement. An approach to transport modeling based on the effects of flow hydraulics on the concentration of suspended and bed load sediments. The Toffaletti equation is more suited for channels in sand beds.

(Fig. 7) depicts the Toffaletti zones for computing sediment transport. This study has two hydrometric stations: one is the Mail Pain, and the second one is the Big Stone Stations. Big Stone Stations are used as the study of upstream and downstream bounds (The River's general schematic is shown in (Fig. 8), while (Fig. 9) presents the cross-section of the study area. The river was divided into 16 sections, each vertical to the river's flow and flowing to the right bank from the left bank. Several cross-sections around the reservoir of the Sadpara dam are utilized. The model's performance for flow simulations was calibrated using the Manning roughness coefficients for the mainstream. For the main channel, 0.05 is the Manning equation's ideal value. (Table 5) shows the coefficients for some commonly used surface materials. (Fig. 10) displays the expected reservoir water surface profiles. In this study, the HEC-RAS model, which had been used to predict sediment loads, determines the geometry of the principal river and reservoir channels. (Fig. 11) is the 3-D flow view, and it is necessary to know the River Hydraulic to compute the sediment movement by HEC-RAS software. To address data limitations, the study made well-justified assumptions to ensure reliability. Manning's roughness coefficient was set at 0.05 based on established ranges and flow simulations. A quasi-unsteady flow method was used in HEC-RAS due to limited high-resolution data. Sediment particle size distributions were derived from regional data, and a rating curve was applied to the downstream boundary. An average sediment load of 230.25 tonnes per day was assumed, supported by field observations and related research. Many sediment transport models use a hydrodynamic simplification technique; however, HEC-RAS employs it. The HEC-RAS model breaks down each steady flow profile into three separate time steps, each subdivision of the previous step to calculate sediment transport. For an upstream external

barrier, a flow series must be chosen based on a computational increment in hours, flow duration in hours, and flow in m^3/s .

3.4 Graphical Results

(Table 5) shows the daily flow rate for a few days of the Sadpara River. Normal Depth, Rating Curve, and Stage Time Series are examples used as downstream boundaries. This investigation uses a "Rating Curve" as the downstream border condition. One option for the boundary condition downstream is a rating curve. The rating curve can be analyzed from (Fig. 12). It is possible to create the Rating Curve (Flow-Stage curve) for the downstream cross-section. It can be analyzed from (Fig. 13) that the Ackers-White equation is best suited for modeling sediment transport and deposition based on sediment particle size mostly due to the large variety of sediment components at different cross sections. From 2012 to 2021, this equation simulates sediment transport and routing. The parameters of the considered model are calibrated to get the best results for the reservoir bed level and deposited sediments. The result is the minimum bed level observed (surveyed) and anticipated for each section along the reservoir. It shows that the HEC-RAS model performs well for both flow and sediment routing scenarios. Most of the sediment load, over 50%, was deposited in Sadpara Dam, which was at the upper half of the reservoir, because of the Deosai River inflow, which carried most of the sediment load entering the reservoir. (Fig. 14) displays the sedimentation profile from 2012 to 2021. For the duration of the investigation, the Deosai River transported 230.25 tons of silt per day on average annually. The lowlands surrounding the reservoir are another place where silt is transported by runoff flow.

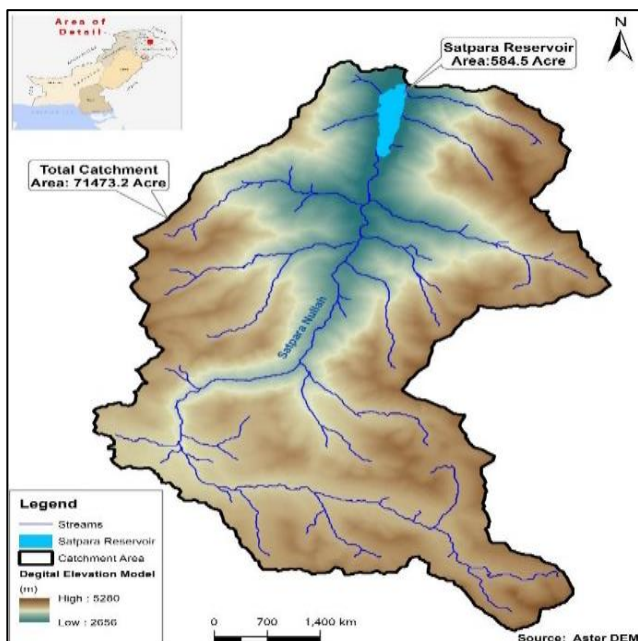


Fig. 1. Hydrology of Sadpara Dam



Fig. 2(a). The reservoir of the Sadpara Dam: Instances of Sedimentation



Fig. 2(b). Effects Of Flood On Sadpara Reservoir

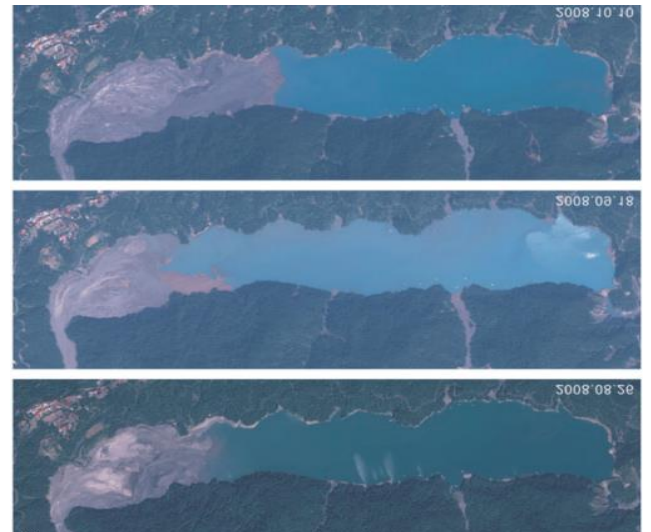


Fig. 3(a). Depicts The Movement Of A Gilbert-Type Delta Into The Wushe Lake In Central Taiwan



Fig. 3(b). Depicts The Movement Of A Gilbert-Type Delta Into The Sadpara Reservoir

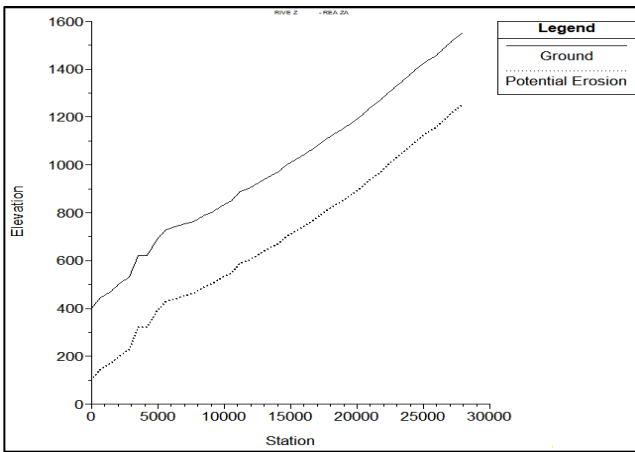


Fig. 4. An illustration of a software menu showing sediment data

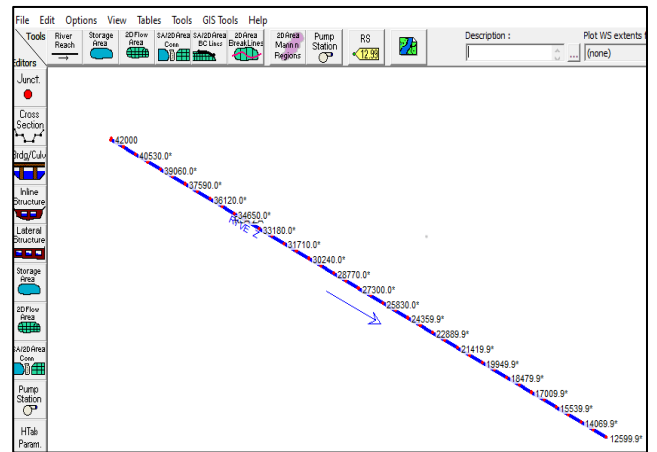


Fig. 8. The River's General Schematic

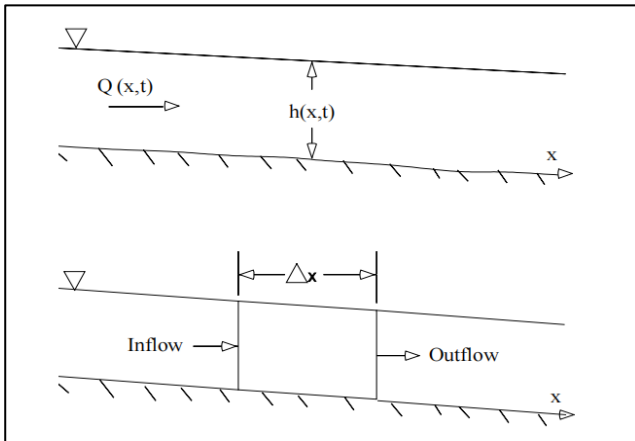


Fig. 5. A General Illustration Of A Cross-Section Of The Continuity Equation

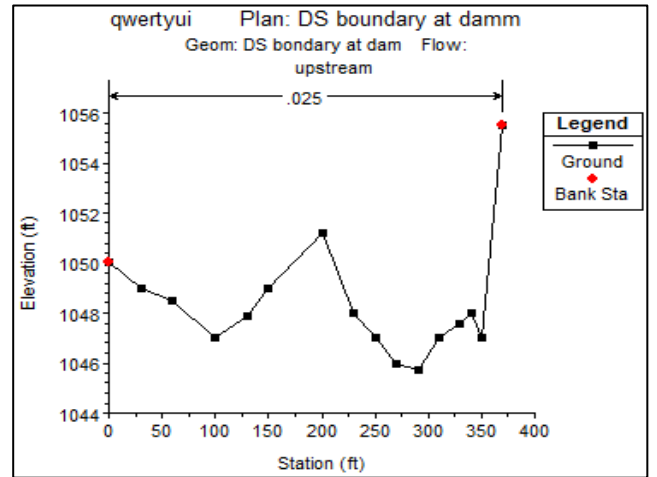


Fig. 9. Cross Section Of The River

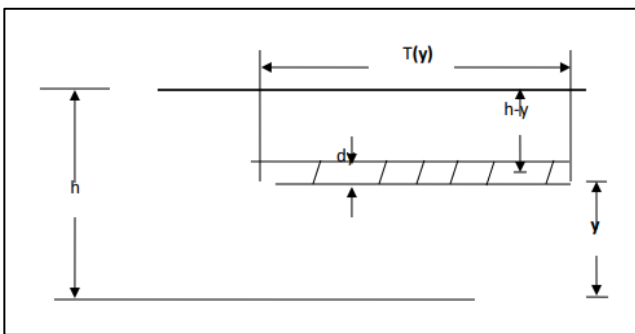


Fig. 6. A General Illustration Of A Cross Section With An Uneven Cross Section Under Pressure

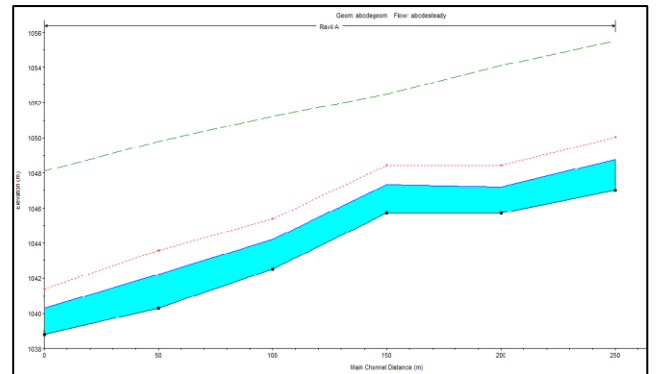


Fig. 10. Water Surface Profile

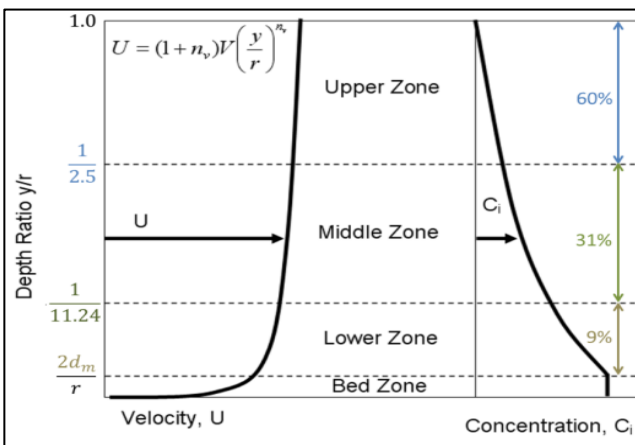


Fig. 7. Toffaleti's zones for computing transport

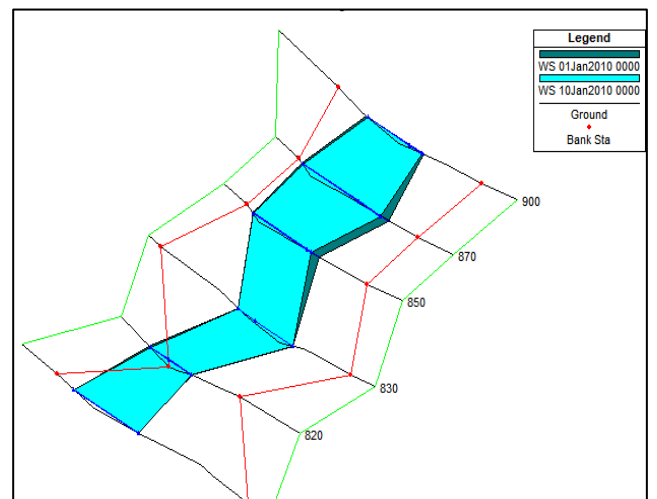


Fig. 11. 3-D Flow View

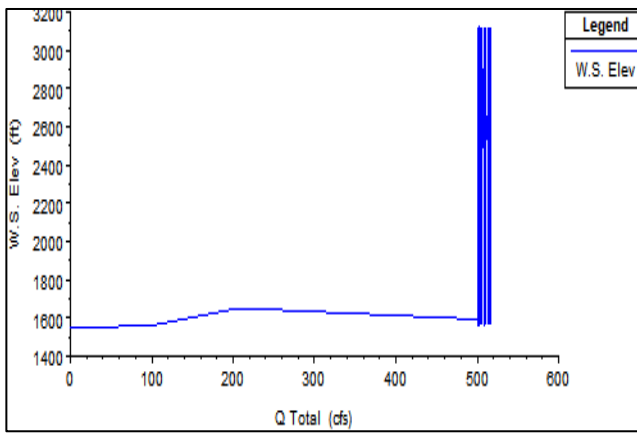


Fig. 12. Rating Curve

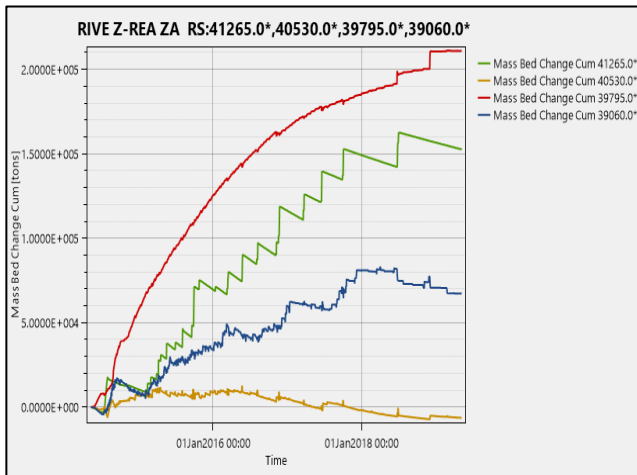


Fig. 13. Sedimentation At Different Stations

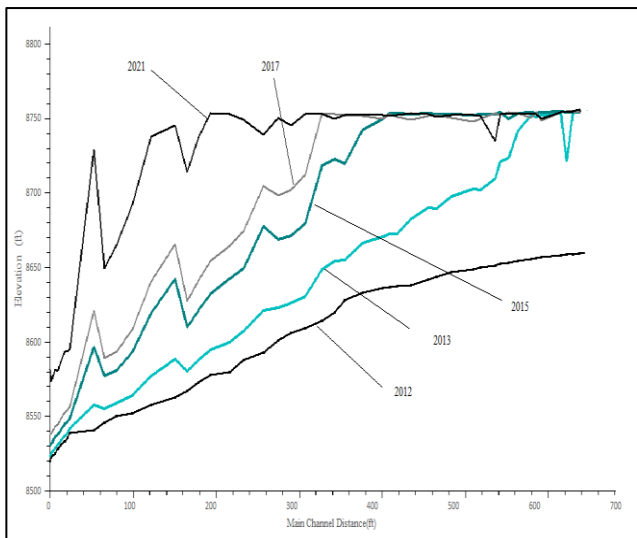


Fig. 14. Sedimentation Profile From 2012 To 2021

4. Conclusion

The Sadpara Dam reservoir's flow and sediment distribution were simulated using the HEC-RAS model. The model was calibrated for flow and sediment deposition from 2014 to 2019. The model simulates the Sadpara river and Sadpara dam because Toffaleti is considered a function for sediment transport for big river systems. The run's most crucial parameter values, for which the preliminary calibration is determined as follows:

Throughout the whole reach, Manning's n varies between 0.03, 0.035, and 0.04 for various river stations.

The sorting algorithm used is Exner and the transport function is Toffaleti.

The 0.062mm to 4mm range of the Toffaleti grain-size validity range corresponded to our final grain sizes, which were used for subsequent validation and calibration.

The obtain results of the study are given as

The findings revealed that runoff flow from the valleys on each side of the reservoir accounted for just around 2.8% of the total annual sediment load of 26.89106 tons.

It should be emphasized that more than half of the sediment was deposited in the upper part of the reservoir, which acts as the principal sediment source, and that most of the material was deposited after the dam began operating.

This modeling has two separate sorts of limitations: those caused by the HEC-RAS model itself and those brought on by a lack of input data which necessitates the use of various simplifications and assumptions. The dredging of accumulated deposits may be done, particularly in the delta region, to change the delta's morphology and decrease the sedimentation of its dead storage capacity. Reducing the amount of silt entering the river from its basin may be possible through watershed management.

In this study only the deosai river water flow is considered to find the sedimentation rate. When Shatong Nullah diverts toward Sadpara Dam, the sedimentation rate also increases, and the 'dam's structure may also affect.

4.1 Future Projection Analysis

While the study includes sedimentation projections until 2060, it does not explicitly account for potential changes due to climate variability. Addressing this requires:

4.2 Incorporating Climate Change Scenarios

Future sedimentation trends depend on changes in glacier melt rates, rainfall intensity, and seasonal flow variations.

Using climate models (e.g., CMIP6 projections) to estimate future inflows from the Deosai River provide a more realistic long-term prediction of sedimentation trends.

4.3 Hydrological Shifts and Their Impact

Increased glacial melt due to rising temperatures may lead to higher sediment loads, accelerating reservoir siltation.

More intense monsoon events could cause short-term spikes in sediment deposition.

Prolonged droughts could reduce flow velocity, allowing more sediment to settle in the reservoir.

4.4 Sediment Management Strategies

Case studies from similar reservoirs experiencing climate-induced sedimentation issues (e.g., Tarbela Dam in Pakistan) provide insights into mitigation strategies.

5. References

- [1] T. M. Abdel-Aziz, "Estimation and prediction of contour maps of Aswan High Dam Reservoir using a two-dimensional model", Proc. 8th Int. Symp. River Sedimentation, Nov. 2001, pp. 3–5.
- [2] G. R. Basson, "Reservoir sedimentation—An overview of global sedimentation rates and predicted sediment deposition", 2008.
- [3] T. Biggs, A. Zeigler, and K. T. Taniguchi-Quan, "Runoff and sediment loads in the Tijuana River: Dam effects, extreme events, and change during urbanization", J. Hydrol. Reg. Stud., vol. 42, p. 101162, 2022.
- [4] F. Behrangi, M. A. Banihashemi, S. Mahani, and M. R. Rahmanian, "Sediment settling in the Latian Dam in Iran", Int. J. Sediment Res., vol. 29, no. 2, pp. 208–217, 2014.
- [5] M. S. El-Sammany and A. M. El-Moustafa, "Adaptation of surface water modeling system for sediment transport investigations in Lake Nasser", J. Nile Basin Water Sci. Eng., vol. 4, no. 1, pp. 71–85, 2011.
- [6] M. El-Moattassem, T. M. Abdel-Aziz, and H. El-Sersawy, "Modeling of sedimentation process in Aswan High Dam Reservoir", Int. Conf. UNESCO Flanders Fit Friend/Nile Project, Towards a Better Cooperation, Sharm El-Sheikh, Egypt, 2005.
- [7] G. A. Fox et al., "Reservoir sedimentation and upstream sediment sources: Perspectives and future research needs on streambank and gully erosion", Environ. Manage., vol. 57, no. 5, pp. 945–955, 2016.
- [8] M. Garcia, Ed., Sedimentation engineering: Processes, measurements, modeling, and practice, American Society of Civil Engineers, May 2008.
- [9] H. Hosseinjanzadeh, K. Hosseini, K. Kaveh, and S. F. Mousavi, "New proposed method for prediction of reservoir sedimentation distribution", Int. J. Sediment Res., vol. 30, no. 3, pp. 235–240, 2015.
- [10] A. H. Haghiabi and E. Zaredehdasht, "Evaluation of HEC-RAS ability in erosion and sediment transport forecasting", World Appl. Sci. J., vol. 17, no. 11, pp. 1490–1497, 2012.
- [11] K. E. Juracek, "The aging of America's reservoirs: In-reservoir and downstream physical changes and habitat implications", JAWRA J. Am. Water Resour. Assoc., vol. 51, no. 1, pp. 168–184, 2015.
- [13] S. Kunwar et al., "Analyzing sedimentation patterns in the Naumure Multipurpose Project (NMP) reservoir using 1D HEC-RAS modeling", Sci. Rep., vol. 14, no. 1, p. 22134, 2024.
- [14] S. Y. Lai and H. Capart, "Reservoir infill by hyperpycnal deltas over bedrock", Geophys. Res. Lett., vol. 36, no. 8, 2009.
- [15] S. Y. Lai and H. Capart, "Reservoir infill by hyperpycnal deltas over bedrock", Geophys. Res. Lett., vol. 36, no. 8, 2009.
- [16] S. Lo Curzio, F. Russo, and M. Caporaso, "Application of remote sensing and GIS analysis to detect morphological changes in an artificial lake", 2013.
- [17] N. Mazhar et al., "Effects of climatic factors on the sedimentation trends of Tarbela Reservoir, Pakistan", SN Appl. Sci., vol. 3, no. 1, pp. 1–9, 2021.
- [18] A. Muhammad and S. M. Ur Rehman, "Multiphase flow simulations through Tarbela Dam spillways and tunnels", J. Water Resour. Prot., vol. 2010, 2010.
- [19] M. Meybeck, "Total mineral dissolved transport by world major rivers/Transport en sels dissous des plus grands fleuves mondiaux", Hydrol. Sci. J., vol. 21, no. 2, pp. 265–284, 1976.
- [20] S. R. Mandwar, H. V. Hajare, and D. A. Gajbhiye, "Assessment of capacity evaluation and sedimentation of Totla Doh Reservoir, in Nagpur district by remote sensing technique", IOSR J. Mech. Civ. Eng., vol. 4, no. 6, pp. 22–25, 2013.

- [21] F. Nu, S. Zhi-Hua, L. Lu, and J. Cheng, "Rainfall, runoff, and suspended sediment delivery relationships in a small agricultural watershed of the Three Gorges area, China", *Geomorphology*, vol. 135, no. 1–2, pp. 158–166, 2011.
- [22] C. A. Obialor et al., "Reservoir sedimentation: Causes, effects and mitigation", *Int. J. Adv. Acad. Res. Sci. Technol. Eng.*, vol. 2488, no. 9849, 2019.
- [23] J. H. Park et al., "Implications of rainfall variability for seasonality and climate-induced risks concerning surface water quality in East Asia", *J. Hydrol.*, vol. 400, no. 3–4, pp. 323–332, 2011.
- [24] C. J. Podolak and M. W. Doyle, "Reservoir sedimentation and storage capacity in the United States: Management needs for the 21st century", *J. Hydraul. Eng.*, vol. 141, no. 4, p. 02515001, 2015.
- [25] A. Rahman, "Sediment management for reservoir", *Proc. Pakistan Eng. Congr.-69 Annu. Session*, 2001–04.
- [25] G. A. Schultz, "Use of remote sensing data in a GIS environment for water resources management", *IAHS Publ.*, vol. 242, pp. 3–16, 1997.
- [26] C. J. Sloff, "Sedimentation in reservoirs", *Commun. Hydraul. Geotech. Eng., Delft Univ. Technol.*, Rep. 97-1, 1997.
- [27] T. Sumi and T. Hirose, "Accumulation of sediment in reservoirs", *Water Storage, Transport, Distrib.*, 2009.
- [28] S. Ren et al., "Sedimentation and its response to management strategies of the Three Gorges Reservoir, Yangtze River, China", *Catena*, vol. 199, p. 105096, 2021.
- [29] W. R. White, *World water: Resources, usage and the role of man-made reservoirs*, 2010.